Supporting Information

Tolerance Factor for Stabilizing 3D Hybrid Halide Perovskitoids Using Linear Diammonium Cations

Xiaotong Li,[†] Mikaël Kepenekian,[§] Linda Li,[‡] Hao Dong,[‡] Constantinos C. Stoumpos, [▽] Ram Seshadri,[◊] Claudine Katan,[§] Peijun Guo, [‡] Jacky Even,[‖] and Mercouri G. Kanatzidis[*,†]

[†]Department of Chemistry, Northwestern University, Evanston, Illinois 60208, United States

[§]Univ Rennes, ENSCR, INSA Rennes, CNRS, ISCR (Institut des Sciences Chimiques de Rennes) - UMR 6226, Rennes F-35000, France

[‡]Department of Chemical and Environmental Engineering, Yale University, New Haven, Connecticut 06511, United States

[▽]Department of Materials Science and Technology, Voutes Campus, University of Crete, Heraklion GR-70013, Greece

[◊]Materials Department and Materials Research Laboratory, University of California, Santa Barbara, California 93106, United States

[‖]Univ Rennes, INSA Rennes, CNRS, Institut FOTON - UMR 6082, Rennes F-35000, France

Powder X-ray Diffraction. Powder X-ray diffraction analysis was performed using a Rigaku Miniflex600 powder X-ray diffractometer (Cu Kα graphite, λ = 1.5406 Å) operating at 40 kV/15 mA with a Kβ foil filter.

Single Crystal Structure. Single-crystal X-ray diffraction experiments were performed using a STOE IPDS II or IPDS 2T diffractometer with Mo Kα radiation (λ = 0.71073 Å) and operating at 50 kV and 40 mA. Integration and numerical absorption corrections were performed using the X-AREA, X-RED, and XSHAPE programs. The structures were solved by charge flipping and refined by full-matrix least-squares on F^2 using the Jana 2006 package.[1] The PLATON software was used to identify the twinning domains and validate the space groups of the compounds.[2]

Computational details. First-principles calculations are based on density functional theory (DFT) as implemented in the SIESTA package.[3,4] Full geometry optimization of the systems, *i.e.* cell vectors and atom positions, have been performed with the nonlocal van der Waals density functional of Dion *et al.* corrected by Cooper (C09),[5,6] without including spin-orbit coupling, until forces were smaller than 0.01 eV/Å. Electronic structure calculations are done including spin-orbit coupling through the on-site approximation as proposed by Fernández-Seivane *et al*.[7] To prevent conflicts between the on-site treatment and the nonlocality of C09, single point calculations are conducted with the revPBE functional on which C09 is based.[8] Core electrons are described with Troullier-Martins pseudopotentials,[9] while valence wavefunctions are developed over double-ζ polarized basis set of finite-range numerical pseudoatomic orbitals.[10] In all cases, an energy cutoff of 150 Ry for real-space mesh size has been used. Complementary calculations for bandgap and defective structures are performed using the HSE06 hybrid functional,[11] including spin-orbit coupling, with the plane-wave projector augmented wave (PAW) method as implemented in the VASP code,[12, 13] using an energy cut-off of 400 eV to expand the electronic wave-functions. Defects in (DMEA)Pb_2Br_6 and (NMPA)Pb_2Br_6 based structures are examined by creating bromide vacancies at different positions (see Figure S1). The geometries are then optimized at the GGA level, while the partial density of states (pDOS) is computed at the HSE level on the relaxed structure.

Optical Absorption Spectroscopy. Optical diffuse reflectance measurements were performed using a Shimadzu UV-3600 UV−vis NIR spectrometer operating in the 200−2500 nm region at room temperature. $BaSO_4$ was used as the reference of 100% reflectance for all measurements.

The reflectance versus wavelength data generated were used to estimate the bandgap of the material by converting reflectance to absorption data according to the Kubelka−Munk equation: $\alpha/S = (1- R)^2(2R)^{-1}$, where R is the reflectance and α and S are the absorption and scattering coefficients, respectively.

Photoluminescence. Photoluminescence was measured using a 375 nm ps laser (Picoquant LDH-D-C-375) as the excitation source running at a 10 MHz repetition rate. A long-working-distance objective (Mitutoyo, 10X, NA=0.28) was used to focus the laser onto the samples and collect the PL signal. The samples were mounted in a liquid-nitrogen cryostat (Janis VPF-100) at a pressure below 10^{-4} Torr. A dichroic mirror was placed on the incident path to block the reflected laser light, and a 400 nm long-pass filter was placed near the entrance slit of the spectrograph (Andor Kymera 328i) to further reject any residual laser light. Time-integrated PL spectra was captured by a Si EMCCD (Andor iXon Life 888), and time-resolved PL was collected by a streak camera (Hamamatsu C10910 with the slow sweep unit; M10913).

Raman Spectra. Low-frequency Raman spectra were measured using a frequency-stabilized 785 nm laser (Toptica) as the excitation source with an incident power of 40 mW onto the sample. A set of 5 narrow-linewidth notch filters (OptiGrate) was used to reject the laser line and enable measurements of Raman signatures down to 5 cm^{-1}. A super-long-working-distance objective lens (10X, NA=0.28) was used to focus the excitation light and to collect the Raman signal. The Raman signal was spatially filtered by a pair of 75-mm achromatic lens and a 50-μm pinhole, before sent into the spectrograph (Andor Kymera 328i). The Raman signal was finally captured by a Si EMCCD (Andor iXon Life 888).

Table S1. Atomic coordinates ($x10^4$) and equivalent isotropic displacement parameters ($Å^2x10^3$) for (1,4BDA)Pb_2Br_6 at 293 K with estimated standard deviations in parentheses.

Label	x	y	z	Occupancy	U_{eq}^*
Pb(1)	2348(1)	6275(1)	5551(1)	1	25(1)
Pb(2)	-2684(1)	6314(1)	5758(1)	1	26(1)
Br(1)	-2591(2)	7855(1)	3944(2)	1	52(1)
Br(3)	-193(2)	6308(1)	5584(2)	1	42(1)
Br(4)	4798(2)	6515(1)	5575(2)	1	40(1)
Br(5)	2780(2)	4578(1)	7133(2)	1	36(1)
Br(6)	2479(2)	5313(1)	2736(2)	1	38(1)
Br(8)	2188(2)	7408(1)	8336(2)	1	52(1)

Table S2. Anisotropic displacement parameters ($Å^2x10^3$) for (1,4BDA)Pb_2Br_6 at 293 K with estimated standard deviations in parentheses.

Label	U_{11}	U_{22}	U_{33}	U_{12}	U_{13}	U_{23}
Pb(1)	22(1)	27(1)	27(1)	0(1)	1(1)	0(1)
Pb(2)	23(1)	29(1)	27(1)	-1(1)	1(1)	-1(1)
Br(1)	57(2)	46(1)	52(1)	-2(1)	-5(1)	22(1)
Br(3)	23(1)	54(1)	48(1)	-2(1)	1(1)	2(1)
Br(4)	23(1)	52(1)	45(1)	-2(1)	2(1)	1(1)
Br(5)	40(1)	41(1)	28(1)	-1(1)	-2(1)	-1(1)
Br(6)	54(1)	34(1)	28(1)	-2(1)	2(1)	-1(1)
Br(8)	61(2)	43(1)	52(1)	0(1)	1(1)	-20(1)

Table S3. Bond lengths [Å] for (1,4BDA)Pb_2Br_6 at 293 K with estimated standard deviations in parentheses.

Label	Distances
Pb(1)-Br(3)	3.0695(18)
Pb(1)-Br(4)	2.9826(18)
Pb(1)-Br(5)	3.1575(17)
Pb(1)-Br(6)	2.9278(15)
Pb(1)-Br(8)	3.0721(17)
Pb(1)-Br(8)#1	2.9093(17)
Pb(2)-Br(3)	3.0148(18)
Pb(2)-Br(4)#2	3.0562(18)
Pb(2)-Br(5)#3	2.9152(15)
Pb(2)-Br(6)#3	2.9953(16)
Pb(2)-Br(1)	2.9986(18)
Pb(2)-Br(1)#4	3.0932(18)

Table S4. Atomic coordinates ($x10^4$) and equivalent isotropic displacement parameters ($Å^2x10^3$) for (NMPA)Pb_2Br_6 at 293 K with estimated standard deviations in parentheses.

Label	x	y	z	Occupancy	U_{eq}*
Pb(1)	4302(1)	3710(1)	5275(3)	1	30(1)
Br(2)	7131(2)	4668(2)	5207(12)	1	39(1)
Br(3)	1199(2)	2823(2)	5295(14)	1	50(1)
Br(4)	4257(2)	3818(2)	442(16)	1	50(1)

Table S5. Anisotropic displacement parameters ($Å^2x10^3$) for (NMPA)Pb_2Br_6 at 293 K with estimated standard deviations in parentheses.

Label	U_{11}	U_{22}	U_{33}	U_{12}	U_{13}	U_{23}
Pb(1)	30(1)	34(1)	26(1)	0(1)	5(1)	-2(2)
Br(2)	31(1)	45(1)	41(2)	4(1)	2(3)	12(3)
Br(3)	47(1)	58(2)	47(2)	-13(1)	-12(3)	-5(4)
Br(4)	51(1)	76(2)	23(3)	-2(1)	-1(2)	1(3)

Table S6. Bond lengths [Å] for (NMPA)Pb_2Br_6 at 293 K with estimated standard deviations in parentheses.

Label	Distances
Pb(1)-Br(2)	2.9911(19)
Pb(1)-Br(2)#1	3.029(2)
Pb(1)-Br(3)	3.139(2)
Pb(1)-Br(3)#2	3.096(2)
Pb(1)-Br(4)	2.922(10)
Pb(1)-Br(4)#3	3.123(10)

Table S7. Atomic coordinates ($x10^4$) and equivalent isotropic displacement parameters ($Å^2x10^3$) for (TMEA)Pb_2Br_6 at 293 K with estimated standard deviations in parentheses.

Label	x	y	z	Occupancy	U_{eq}*
Pb(1)	4409(1)	2897(1)	8827(2)	1	27(1)
Br(2)	3830(1)	5862(2)	8731(6)	1	50(1)
Br(3)	5000	0	8726(6)	1	65(1)
Br(5)	2500	2379(2)	9072(6)	1	50(1)
Br(7)	4366(2)	2954(2)	3798(6)	1	56(1)

Table S8. Anisotropic displacement parameters ($Å^2x10^3$) for (TMEA)Pb_2Br_6 at 293 K with estimated standard deviations in parentheses.

Label	U_{11}	U_{22}	U_{33}	U_{12}	U_{13}	U_{23}
Pb(1)	28(1)	24(1)	30(1)	0(1)	-2(1)	4(1)
Br(2)	34(1)	31(1)	84(2)	2(1)	-6(3)	-5(3)
Br(3)	81(2)	33(1)	80(2)	19(1)	0	0
Br(5)	31(1)	45(2)	73(2)	0	0	1(2)
Br(7)	78(1)	63(1)	28(1)	9(1)	4(3)	2(3)

Table S9. Bond lengths [Å] for (TMEA)Pb_2Br_6 at 293 K with estimated standard deviations in parentheses.

Label	Distances
Pb(1)-Br(2)	3.0350(18)
Pb(1)-Br(2)#1	2.9812(18)
Pb(1)-Br(3)	2.9775(12)
Pb(1)-Br(5)	2.9960(13)
Pb(1)-Br(7)	3.068(4)
Pb(1)-Br(7)#2	3.033(4)

Table S10. Atomic coordinates ($x10^4$) and equivalent isotropic displacement parameters ($Å^2x10^3$) for (DMEA)Pb_2Br_6 at 293 K with estimated standard deviations in parentheses.

Label	x	y	z	Occupancy	U_{eq}^*
Pb(1)	1023(1)	7006(1)	1502(1)	1	26(1)
Pb(2)	-1192(1)	8169(1)	3243(1)	1	27(1)
Br(3)	-361(2)	6380(1)	2749(2)	1	34(1)
Br(4)	2254(2)	7662(2)	2881(2)	1	34(1)
Br(5)	91(2)	8704(1)	1690(2)	1	37(1)
Br(6)	2559(2)	7712(1)	383(1)	1	32(1)
Br(7)	1835(2)	5049(2)	1718(2)	1	48(1)
Br(8)	98(2)	6520(2)	-237(2)	1	66(1)

Table S11. Anisotropic displacement parameters ($Å^2x10^3$) for (DMEA)Pb_2Br_6 at 293 K with estimated standard deviations in parentheses.

Label	U_{11}	U_{22}	U_{33}	U_{12}	U_{13}	U_{23}
Pb(1)	27(1)	25(1)	26(1)	0(1)	1(1)	0(1)
Pb(2)	25(1)	28(1)	27(1)	1(1)	1(1)	0(1)
Br(3)	36(1)	28(1)	36(1)	0(1)	4(1)	5(1)
Br(4)	40(1)	40(1)	24(1)	-3(1)	0(1)	1(1)
Br(5)	46(1)	28(1)	38(1)	6(1)	4(1)	8(1)
Br(6)	38(1)	36(1)	24(1)	-2(1)	-2(1)	0(1)
Br(7)	65(2)	30(1)	51(2)	0(1)	11(2)	-1(1)
Br(8)	49(2)	98(2)	52(2)	9(2)	-17(2)	-14(2)

Table S12. Bond lengths [Å] for (DMEA)Pb_2Br_6 at 293 K with estimated standard deviations in parentheses.

Label	Distances
Pb(1)-Br(3)	2.990(2)
Pb(1)-Br(4)	2.9892(19)
Pb(1)-Br(5)	2.9200(19)
Pb(1)-Br(6)	3.079(2)
Pb(1)-Br(7)	3.194(2)
Pb(1)-Br(8)	3.107(3)
Pb(2)-Br(3)	3.0545(19)
Pb(2)-Br(4)#1	3.016(2)
Pb(2)-Br(5)	3.182(2)
Pb(2)-Br(6)#1	2.9168(19)
Pb(2)-Br(7)#2	2.977(2)
Pb(2)-Br(8)#3	3.081(3)

Table S13. Dimensions of the A-cations extracted from single-crystal structures. (Structures 3-8 were reported in the literature.[14])

	A-cation	L_x < 5.27 Å	L_y < 9.72 Å	L_z < 2.66 Å
(1,4BDA)Pb_2Br_6	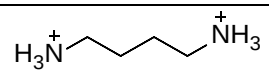	2.27	7.49	2.27
(NMPA)Pb_2Br_6	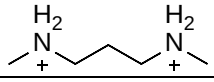	2.27	8.33	2.27
(1,3PDA)Pb_2Br_6	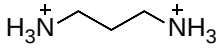	2.27	6.13	2.27
(DMPZ)Pb_2Br_6	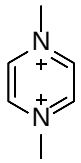	3.72	7.04	1.40
(HMPZ)Pb_2Br_6	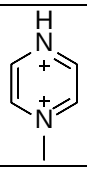	3.70	6.28	1.40
(HEPZ)Pb_2Br_6	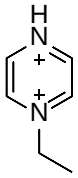	3.75	6.67	2.40
(HPPZ)Pb_2Br_6	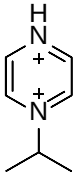	3.73	6.29	3.93
(H_2APY)Pb_2Br_6	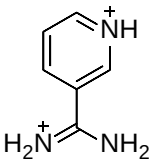	3.77	6.22	2.50

Table S14. Lifetime fitting parameters for (1,4BDA)Pb_2Br_6 at different temperatures.

T	a_1	τ_1	a_2	τ_2	τ_{ave}
215 K	0.99	0.12	0.01	1.75	0.13
175 K	0.98	0.16	0.02	2.10	0.19
135 K	0.98	1.16	0.02	13.10	1.37
78 K	0.41	13.63	0.59	66.26	44.49

Table S15. Lifetime fitting parameters for (NMPA)Pb_2Br_6 at different temperatures.

T	a_1	τ_1	a_2	τ_2	τ_{ave}
215 K	0.01	4.41	0.99	0.88	0.91
175 K	0.66	5.89	0.34	22.18	11.42
135 K	0.25	67.46	0.75	210.38	174.38
78 K	0.29	324.78	0.71	811.49	670.38

Table S16. Lifetime fitting parameters for (TMEA)Pb_2Br_6 at different temperatures.

T	a_1	τ_1	a_2	τ_2	τ_{ave}
135 K	0.99	0.52	0.01	5.85	0.56
78K	0.99	2.14	0.01	14.94	2.19

Table S17. Lifetime fitting parameters for (DMEA)Pb_2Br_6 at different temperatures.

T	a_1	τ_1	a_2	τ_2	τ_{ave}
295 K	0.84	0.54	0.16	4.54	1.19
255 K	0.74	0.16	0.26	2.66	0.81
215 K	0.63	3.33	0.37	21.98	10.29
175 K	0.99	10.45	0.01	200.94	12.64
135 K	0.97	11.39	0.03	200.64	17.18
78 K	0.76	63.45	0.24	393.29	141.65

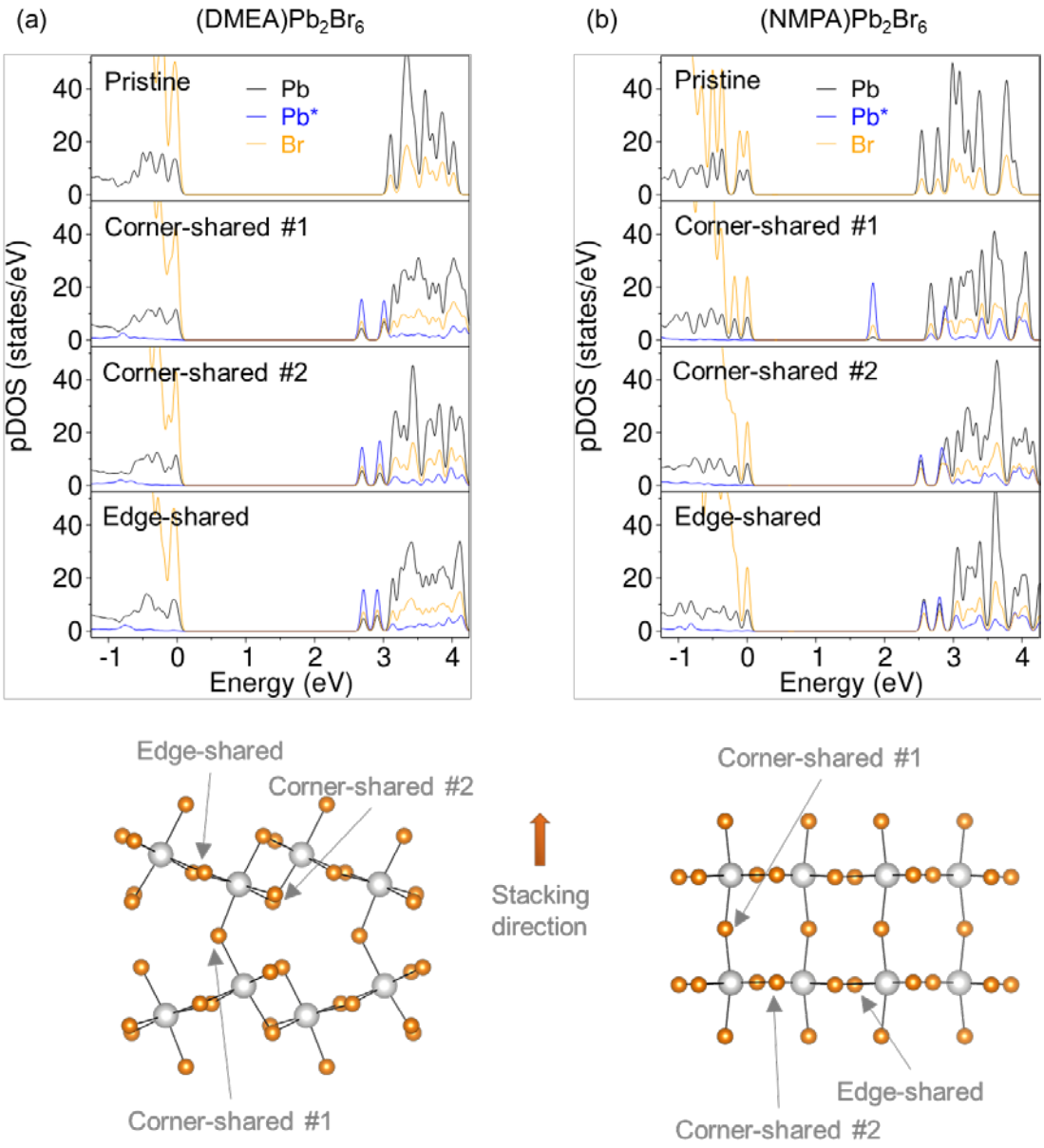

Figure S1. Partial density of states (pDOS) computed at the HSE level for (a) $(DMEA)Pb_2Br_6$ and (b) $(NMPA)Pb_2Br_6$ on structures relaxed (at the GGA level) with different bromide vacancies, which are illustrated below the corresponding panels. When bromine vacancies were generated at different positions, below-bandgap trap states showed up at different energies. The black lines indicate the pDOS of pristine Pb. The blue lines indicate the pDOS of Pb surrounded by Br vacancies. The orange lines are the pDOS of Br.

References

[1] Petříček, V.; Dušek, M.; Palatinus, L., Crystallographic Computing System JANA2006: General features. Z. Kristallogr. - Cryst. Mater. 2014, 229 (5), 345.

[2] Spek, A., Structure validation in chemical crystallography. Acta Crystallogr. D 2009, 65 (2), 148.

[3] Soler, J. M.; Artacho, E.; Gale, J. D.; García, A.; Junquera, J.; Ordejón, P.; Sánchez-Portal, D. The SIESTA method for ab initio order-N materials simulation. *J. Phys.: Condens. Matter* **2002**, *14*, 2745.

[4] Artacho, E.; Anglada, E.; Diéguez, O.; Gale, J. D.; García, A.; Junquera, J.; Martin, R. M.; Ordejón, P.; Pruneda, J. M.; Sánchez-Portal, D. ; Soler, J. M. The SIESTA method; developments and applicability. *J. Phys.: Condens. Matter* **2008**, *20*, 064208.

[5] Dion, M.; Rydberg, H.; Schröder, E.; Langreth, D. C.; Lundqvist, B. I. Van der Waals Density Functional for General Geometries. *Phys. Rev. Lett.* **2004**, *92*, 246401.

[6] Cooper, V. R. Van der Waals density functional: An appropriate exchange functional. *Phys. Rev. B: Condens. Matter Mater. Phys.* **2010**, *81*, 161104.

[7] Fernández-Seivane, L.; Oliveira, M. A.; Sanvito, S.; Ferrer, J. On-site approximation for spin–orbit coupling in linear combination of atomic orbitals density functional methods. *J. Phys.: Condens. Matter* **2006**, *18*, 7999.

[8] Zhang, Y.; Yang, W. Comment on "Generalized Gradient Approximation Made Simple". *Phys. Rev. Lett.* **1998**, *80*, 890.

[9] Troullier, N.; Martins, J. L. Efficient pseudopotentials for plane-wave calculations. *Phys. Rev. B* **1991**, *43*, 1993.

[10] Artacho, E.; Sánchez-Portal, D.; Ordejón, P.; García, A.; Soler, J. M. Linear-Scaling ab-initio Calculations for Large and Complex Systems. *Phys. Stat. Sol. (b)* **1999**, *215*, 809.

[11] Aliaksandr V. Krukau, Oleg A. Vydrov, Artur F. Izmaylov, and Gustavo E. Scuseria. Influence of the exchange screening parameter on the performance of screened hybrid functionals, *J. Chem. Phys.* **2006**, *125*, 224106.

[12] Kresse, G.; Furthmüller, J., Efficient iterative schemes for ab initio total-energy calculations using a plane-wave basis set. *Phys. Rev. B* **1996**, 54 (16), 11169.

[13] Kresse, G.; Furthmüller, J., Efficiency of ab-initio total energy calculations for metals and semiconductors using a plane-wave basis set. *Comput. Mater. Sci.* **1996**, 6 (1), 15.

[14] Umeyama, D.; Leppert, L.; Connor, B.; Manumpil, M. A.; Neaton, J.; Karunadasa, H., Expanded Analogs of Three-Dimensional Lead-Halide Hybrid Perovskites. Angew. Chem., Int. Ed. 2020, 59 (43), 19087.